An Application-Oriented Approach for Consideration of Material Degradation Effects Due to Cutting on Iron Losses and Magnetizability

Simon Steentjes, Georg von Pfingsten, and Kay Hameyer

Institute of Electrical Machines, RWTH Aachen University, Aachen D-52056, Germany

The decrease in magnetic permeability and increase of local hysteresis loss in the vicinity of lamination edges originating from the cutting process need to be accounted for during the design of electrical machines. A flexible method is needed, which is able to account for different degradation profiles due to different cutting techniques. This paper presents a quantitative analysis of the impact of material degradation on iron losses and magnetizability due to guillotine shear and CO_2 laser cutting for non-oriented electrical steels.

Index Terms— **Ferromagnetic material modeling, iron losses, magnetic hysteresis, material degradation, non-oriented electrical steel (NOES).**

I. Introduction

NON-ORIENTED electrical steel (NOES) used in traction drives is mainly characterized by its magnetic properties, i.e., the specific iron loss P_{fe}, magnetic saturation polarization J_s, and permeability. In addition, mechanical properties, e.g., manufacturability, yield strength, and coatings become more and more important since they strongly influence the power density and cost of the resulting electric machine.

A negative side effect of material processing is the decrease in magnetic permeability [1] and increase of local hysteresis loss [1] in the vicinity of lamination edges.

The reason for this is related to local detrimental changes in the micro-structure of the electrical steel, such as dislocations, internal stresses, and grain morphology. These adverse influences need to be accounted for during the design of electrical machines.

Currently, these effects, to the greatest possible extent, are studied qualitatively and included in the design process using building factors [2]; however, just a few attempts are made to include the occurring material degradation effects in the simulation process [3]–[5].

In addition, knowledge on the correlation of material processing steps and magnetic material properties is indispensable to fine-tune not only the material processing itself, as for instance, the cold-rolling process or the cutting process parameters [1], but also the material composition [6].

This paper presents a pragmatic modeling approach that enables us to consider the effect of material degradation on magnetizability and iron losses of soft magnetic materials. The paper is structured as follows. Section II briefly dwells on the sample preparation and metrological characterization. Furthermore, an evaluation of the iron-loss increase due to cutting and increased need of magnetic field strength to reach a particular magnetic polarization level in samples with an increased proportion of degraded zone is presented. Section III introduces the main modeling approach to describe the local magnetization behavior together with exemplary results for a 2.4% Si NOES grade. Section IV presents a pragmatic approach to include the increased iron losses due to cutting. Finally, Section V provides a discussion of the results and points out the scope for future work.

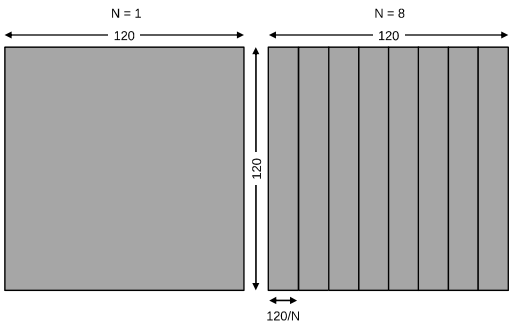

Fig. 1. Exemplary sample sets. Left: Uncut 120 × 120 mm sample. Right: Sample set consisting of eight ($N = 8$) $b = 15$ mm wide stripes ($b = 120/\mathrm{N}$) of 120 mm length lined up to reach an overall width of 120 mm.

II. Sample Sets and Metrological Characterization

To study the influence of material degradation due to various cutting techniques, material characteristics are measured for sample sets with different ratios of cut surface versus overall lamination volume, i.e., with different proportions of the degraded zone, as in [7] and [8].

Therefore, several 500 mm × 500 mm samples of 2.4 wt% Si NOES of thickness 0.3 mm are taken from different positions in a cold-rolled stripe. To ensure that the different base materials are magnetically equivalent, metrological characterizations of the samples using unidirectional, sinusoidal magnetic flux density waveforms are conducted. A deviation of less than 1% between the values of different samples both along and perpendicular to the rolling direction confirms the homogeneity of the studied materials.

Starting from this base material, a number of single sheet tester (SST) samples of 120 mm × 120 mm are cut into smaller stripes by guillotine shear cutting (simulating the actual punching) others by CO_2 laser cutting (Fig. 1).

Some of the samples do not have overlapping degraded zones, i.e., have degraded zones smaller than the half stripe

Manuscript received March 8, 2014; revised June 20, 2014; accepted June 22, 2014. Date of current version November 18, 2014. Corresponding author: S. Steentjes (e-mail: simon.steentjes@iem.rwth-aachen.de).

Color versions of one or more of the figures in this paper are available online at http://ieeexplore.ieee.org.

Digital Object Identifier 10.1109/TMAG.2014.2334699

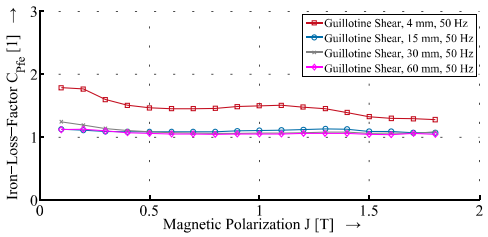

Fig. 2. Iron-loss increase due to a decreasing single stripe width, i.e., increasing proportion of the degraded zone, at 50 Hz for a 2.4 wt% Si NOES with guillotine shear cut samples.

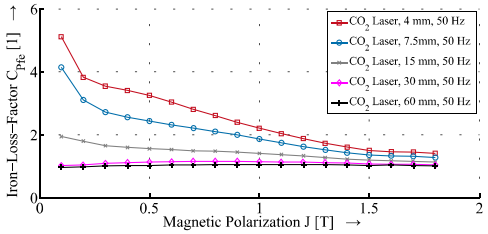

Fig. 3. Iron-loss increase due to a decreasing single stripe width at 50 Hz, i.e., increasing proportion of the degraded zone, for a 2.4 wt% Si NOES grade with CO_2 laser cut samples.

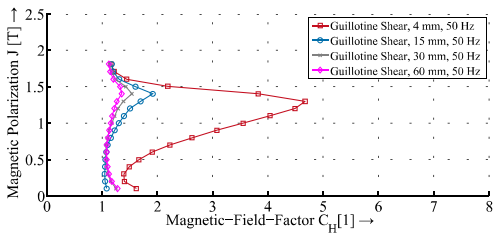

Fig. 4. Increase of required magnetic field strength to reach a particular magnetic polarization level at 50 Hz in sample sets consisting of N single stripes of different widths b cut by guillotine shear for a 2.4 wt% Si NOES grade.

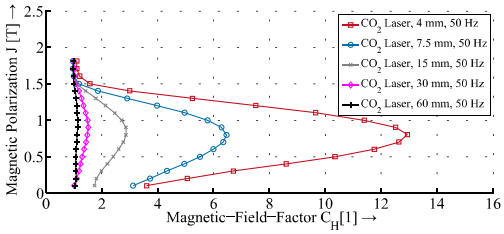

Fig. 5. Increase of required magnetic field strength to reach a particular magnetic polarization level at 50 Hz in sample sets consisting of N single stripes of different widths b cut by CO_2 laser for a 2.4 wt% Si NOES grade.

width, and therefore unaffected material in the center of the sample. Others have overlapping degraded zones.

The sample sets consisting of N smaller stripes are lined up and fixed by a non-magnetic adhesive tape to yield sample sets with a total width of 120 mm (Fig. 1), which are characterized in the 120 mm × 120 mm SST [9]. Measurements are performed utilizing the field-metric method [9] under sinusoidal magnetic flux densities up to high amplitudes at 50 Hz. For clarity, in this paper, merely results for measurements in rolling direction are presented. Perpendicular to the rolling direction, the cutting effect is less pronounced.

Figs. 2 and 3 give an overview of the change of the iron-loss measured along the rolling direction with respect to the single stripe width of one sample set (Fig. 1). To study the differences resulting from different single stripe widths and cutting methods, a factor is defined: the iron-loss factor C_{Pfe}.

This factor represents the ratio between measured losses in the sample set consisting of N single stripes of smaller width b and the uncut sample set of 120 mm width

$$C_{\mathrm{Pfe}}(J, f, b) = \frac{P_b(J, f)}{P_{120\ \mathrm{mm}}(J, f)} \tag{1}$$

where b represents the width of a single stripe of the complete sample set under study (Fig. 1). For instance, factor 5 in Fig. 3 means that the iron-loss at a polarization of 0.1 T is five times larger in 30 stripes each CO_2 laser cut of 4 mm width than in one stripe of 120 mm width.

Figs. 4 and 5 depict the increase of magnetic field strength in the sample set consisting of N single stripes of smaller width b, which is required to reach the same magnetic polarization level as in the uncut sample set of 120 mm width. Therefore, a magnetic field factor C_H is defined as

$$C_H(J, f, b) = \frac{H_b(J, f)}{H_{120\ \mathrm{mm}}(J, f)}. \tag{2}$$

It is apparent that for increasing magnetic polarizations, the material degradation effects get less significant (Figs. 4 and 5).

III. Local Magnetization Behavior

Due to cutting, a spatial distribution of magnetic polarization $J(x)$ as function of the distance x to the cut edge is present. Thereby, it is important to emphasize that measured magnetic polarizations represent a mean value across the samples' cross section. A non-uniform flux distribution over the width of the sample originates from the degraded properties at the cut surface.

Micromagnetic measurements reported in [10] show that the spatial distribution in case of guillotine shear cutting is parabolic and can have a depth, depending on its definition, of up to 10 mm [1], [10], and [11]. However, recent studies for different laser cutting techniques enabling neutron grating interferometry point toward other degradation profiles [12].

In case of laser cutting, the absorption of laser power in combination with the thermal conductivity of the material leads to thermal deterioration. Across the heat-affected zone, elastic and plastic deformations or even phase transformation can occur. These deformations change the residual stress state; hence the degradation could be attributed to induced internal biaxial stresses. Therefore, a flexible methodology is needed that is able to account for different degradation profiles due to various cutting techniques [1], [10]–[12].

The approach proposed in [13] offers the sought for flexibility. The homogeneity of the magnetic field strength H over the sample enables a consideration of the material degradation as a local inhomogeneous decrease of the magnetic permeability μ, noted as $\Delta\mu(H, x)$ [13].

According to [13], the increase of microstructural defects at the cut surface and the corresponding maximal permeability drop $\Delta\mu_{\mathrm{cut}}(H) = \Delta\mu(H, x = 0)$ are assumed to be material constants. Hence, the spatial distribution of $\Delta\mu(H, x)$ can be expressed in terms of a field-independent spatial distribution function $\eta(x)$ [13]. This field-independent spatial distribution function relates to the degradation profile, which could be identified based on the calculation of induced plastic deformation [3], [14],

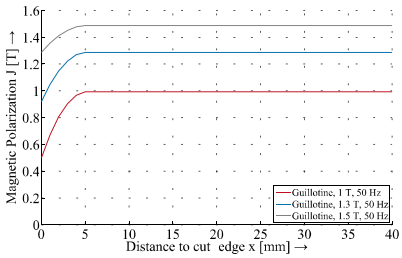

Fig. 6. Magnetic polarization J[T] as a function of the distance to the cut edge x[mm] for guillotine shear cut samples.

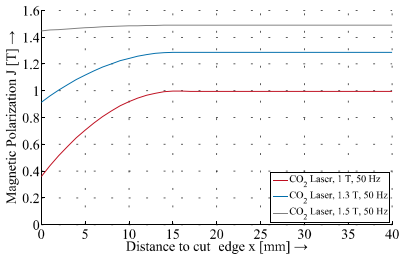

Fig. 7. Magnetic polarization J[T] as a function of the distance to the cut edge x[mm] for CO_2 laser cut samples.

the distribution of thermal induced stresses due to various laser cutting methods or based on assumptions for a stable Finite-Element simulation [15].

Because of the homogeneity of the magnetic field strength across the samples' cross section, this spatial distribution relates to that of the magnetic polarization [13]. Therewith it is possible to reconstruct the magnetic polarization distribution as a function of the distance to the cut edge.

Here, due to the lack of experimental data, a parabolic distribution of the magnetic polarization as a function of the distance to the cut edge is assumed [8], [9] for both studied cutting techniques.

Figs. 6 and 7 show the obtained results according to [13] of the local distribution of the magnetic polarization for stripes cut by a guillotine shear and a CO_2 laser beam. It is apparent that in case of CO_2 laser cutting, a significantly larger degraded zone appears compared with the guillotine shear cut.

IV. Iron-Loss Modeling Approach

In the following, an approach to consider the increased iron losses (Figs. 2 and 3) will be introduced. Therefore, the impact of cutting is implemented into the coefficients of a state-of-the-art iron-loss formula (3)–(6) [13], [16], which was developed to predict the iron losses at higher magnetic polarization levels and higher frequencies more accurately

$$P_{\mathrm{Pfe}}(\hat{B}, f, x) = P_{\mathrm{hy}}(\hat{B}, f, x) + P_{\mathrm{cl}}(\hat{B}, f, x) + P_{\mathrm{exc}}(\hat{B}, f, x) + P_{\mathrm{sat}}(\hat{B}, f, x)$$

including hysteresis loss P_{hy}, Foucault eddy current loss P_{cl}, excess eddy current loss P_{exc}, and saturation eddy current loss P_{sat}

$$P_{\mathrm{hy}}(\hat{B}(x), f) = a_1\left(1 + \frac{B_{\min}}{B_{\max}}(r_{\mathrm{hy}}(\hat{B}(x)) - 1)\right)\hat{B}(x)^{\alpha} f \quad (3)$$

$$P_{cl}(\hat{B}(x), f) = a_2 \sum\nolimits_{n=0}^{\infty} \left(\hat{B}(x)_n^2 f_n^2\right) \quad (4)$$

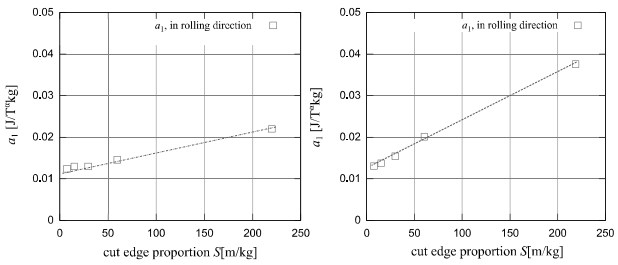

Fig. 8. Parameter a_1 as a function of the cut edge proportion with $\alpha = 1.8$. Left: Guillotine shear cut samples in rolling direction. Right: CO_2 laser cut samples.

$$P_{\mathrm{exc}}(\hat{B}(x), f) = a_5\left(1 + \frac{B_{\min}}{B_{\max}}(r_{\mathrm{exc}}(\hat{B}(x)) - 1)\right) \times \sum\nolimits_{n=0}^{\infty} \left(\hat{B}(x)_n^2 f_n^2\right)^{0.75} \quad (5)$$

$$P_{\mathrm{sat}}(\hat{B}(x), f) = a_2 a_3 \hat{B}(x)^{a_4+2} f^2. \quad (6)$$

It is assumed that the quasi-static hysteresis losses are most prone to cutting, corroborated by the behavior of the coercive field $H_c(H)$ and quasi-static hysteresis loops $J(H)$ [13]. Hence, parameter a_1 related to pure hysteresis loss (3) is adapted to account for an increased proportion of the degraded zone. Parameter α is kept constant to 1.8, resulting in best agreements between measured quasi-static hysteresis loss and estimated ones.

In addition, it is supposed that the chemical composition, and consequently, the specific electrical resistivity are locally not influenced by the cutting process. Hence, the classical induced eddy currents (4) are not directly influenced by the cutting technique, only their distribution will (indirectly) be affected by the cut surface properties. This is due to the aforementioned variation of the local magnetic polarization J. Further on, the saturation behavior of the magnetization process is assumed to be uninfluenced. Hence, losses due to material saturation (6) are not affected.

The degrading effect on iron losses is described by the cutting strains defined by Hribernik as the cutting surface $A(\mathrm{m}^2)$ referenced to the sample volume $V(\mathrm{m}^3)$ [18]. Assuming constant thickness and specific density, the cutting strains can be expressed as cut edge length l_{cut} per unit mass m_s, named cut edge proportion S[m/kg].

As a first step, parameter a_1 is identified for each sample set using point-by-point dc-measurements, which allows a determination of a_1 solely [17]. Fig. 8 shows the obtained parameters as a function of the cut edge proportion S [18]. A linear relation is apparent for both cutting techniques. Comparing the slopes of the interpolated curves for the CO_2 laser and guillotine shear cut sample sets, it is apparent that the increase of hysteresis loss, directly correlating with coefficient a_1, in case of CO_2 laser cutting is much more significant. This is in line with the estimated local flux density distribution (Figs. 6 and 7).

As a result, the hysteresis loss component (3) is rewritten as

$$P_{\mathrm{hy}}\big(\hat{B}(x), f\big) = a_1(S)\Big(1 + \frac{B_{\min}}{B_{\max}}(r_{\mathrm{hy}}\big(\hat{B}(x)\big) - 1)\Big)\hat{B}(x)^{\alpha} f. \quad (7)$$

In this hysteresis loss description, the hysteresis coefficient a_1 is dependent on the cut edge proportion S

$$a_1(S) = a_{1;\mathrm{ref}} + d\big(S - S_{\mathrm{ref}}\big) \quad (8)$$

where d is the gradient of the linear equation, which could be determined by a line of best fit through the estimated

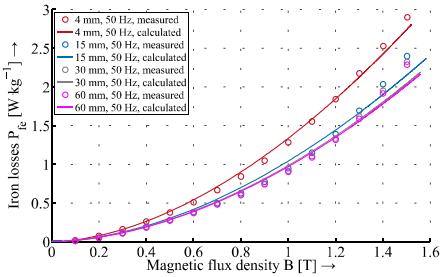

Fig. 9. Specific iron losses P_{fe}[W/kg] as a function of the magnetic flux density for a 2.4 wt% Si NOES grade at 50 Hz excitation frequency for guillotine cut samples.

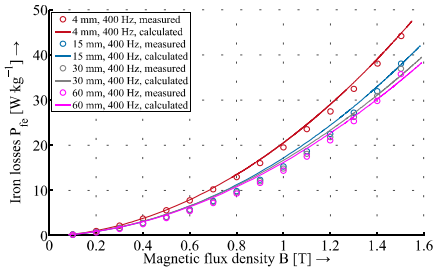

Fig. 10. Specific iron losses P_{fe}[W/kg] as a function of the magnetic flux density for a 2.4 wt% Si NOES grade at 400 Hz excitation frequency for guillotine shear cut samples.

a_1-parameters of different sample sets. $a_{1;\mathrm{ref}}$ is the hysteresis loss parameter of the reference sample set with the corresponding reference cut edge proportion S_{ref}.

Therewith it is possible to calculate the iron loss in stripes of any width at least from two parameter sets a_1 and S, for instance, using the parameter set of the uncut sample as a reference ($a_{1;\mathrm{ref}} = a_{1;120\ \mathrm{mm}}$ and $S_{\mathrm{ref}} = l_{\mathrm{cut};120\ \mathrm{mm}}/m_{s;120\ \mathrm{mm}}$) combined with a_1 and S of any sample set consisting of N smaller stripes to determine the slope ($a_{1;b}$ and $S_b = l_{\mathrm{cut};b}/m_{s;b}$).

This model is subsequently applied to calculate iron losses in sample sets consisting of guillotine shear cut stripes of width b. Fig. 9 presents the obtained loss predictions at 50 Hz and Fig. 10 for an excitation frequency of 400 Hz.

The accuracy is sufficient for various stripe sizes, i.e., different proportions of degraded zone, using just two measured sample sets with adequate difference in their cut edge proportion for parameterization. The relative deviation is always less than 10% for both cutting methods.

V. Conclusion

The phenomenon of iron-loss increase and local magnetic polarization profiles due to guillotine shear and CO_2 laser cutting of electrical steel laminations has been characterized in case of a 2.4 wt% Si NOES grade. A flexible methodology to account for the local magnetization distribution has been applied. Different sizes of degraded zones depending on the cutting method are observed emphasizing the need for a thorough investigation.

Further on, cutting increases the iron loss due to two phenomena. On the one hand by modifying the magnetization profile and on the other hand due to the increase of hysteresis loss through modifications in the micro-structure and stress state of the material. To account for this, a method based on the influence of induced cutting strains is used and validated by measurements.

Future work will focus on an inclusion of the local change of the shape of the hysteresis loop in the aforementioned iron-loss model, i.e., in parameter a_1.

Acknowledgment

This work was supported by the Deutsche Forschungsgemeinschaft and carried out in the research project improved modeling and characterization of ferromagnetic materials and their losses.

References

[1] P. Baudouin, M. De Wulf, L. Kestens, and Y. Houbaert, "The effect of the guillotine clearance on the magnetic properties of electrical steels," *J. Magn. Magn. Mater.*, vol. 256, nos. 1–3, pp. 32–40, 2003.

[2] G. Müller, K. Vogt, and B. Ponick, *Berechnung Elektrischer Maschinen*. New York, NY, USA: Wiley, 2008.

[3] F. Ossart, E. Hug, O. Hubert, C. Buvat, and R. Billardon, "Effect of punching on electrical steels: Experimental and numerical coupled analysis," *IEEE Trans. Magn.*, vol. 36, no. 5, pp. 3137–3140, Sep. 2000.

[4] Z. Gmyrek and A. Cavagnino, "Analytical method for determining the damaged area width in magnetic materials due to punching process," in *Proc. 37th Annu. Conf. IEEE Ind. Electron. Soc. (IECON)*, Nov. 2011, pp. 1764–1769.

[5] W. M. Arshad *et al.*, "Incorporating lamination processing and component manufacturing in electrical machine design tools," in *Proc. 42nd IAS Annu. Meeting Conf. Rec. IEEE Ind. Appl. Conf. (IAS)*, Sep. 2007, pp. 94–102.

[6] P. Baudouin, A. Belhadj, F. Breaban, A. Defontaine, and Y. Houbaert, "Effects of laser and mechanical cutting modes on the magnetic properties of low and medium Si content non-oriented electrical steels," *IEEE Trans. Magn.*, vol. 38, no. 5, pp. 3213–3215, Sep. 2002.

[7] K.-H. Schmidt, "Influence of punching on the magnetic properties of electric steel with 1% silicon," *J. Magn. Magn. Mater.*, vol. 2, nos. 1–3, pp. 136–150, Feb. 1976.

[8] A. Schoppa, J. Schneider, and C. D. Wuppermann, "Influence of the manufacturing process on the magnetic properties of non-oriented electrical steels," *J. Magn. Magn. Mater.*, vols. 215–216, pp. 74–78, Jun. 2000.

[9] F. Fiorillo, *Characterization and Measurement of Magnetic Materials*. New York, NY, USA: Academic, 2004.

[10] T. Nakata, M. Nakano, and K. Kawahara, "Effects of stress due to cutting on magnetic characteristics of silicon steel," *IEEE Transl. J. Magn. Jpn.*, vol. 7, no. 6, pp. 453–457, Jun. 1992.

[11] A. J. Moses, N. Derebasi, G. Loisos, and A. Schoppa, "Aspects of the cut-edge effect stress on the power loss and flux density distribution in electrical steel sheets," *J. Magn. Magn. Mater.*, vols. 215–216, pp. 690–692, Jun. 2000.

[12] R. Siebert, A. Wetzig, E. Beyer, B. Betz, C. Grünzweig, and E. Lehmann, "Localized investigation of magnetic bulk property deterioration of electrical steel: Analysing magnetic property drop thorough mechanical and laser cutting of electrical steel laminations using neutron grating interferometry," in *Proc. 3rd Int. Electr. Drives Product. Conf. (EDPC)*, 2013, pp. 1–5.

[13] L. Vandenbossche, S. Jacobs, F. Henrotte, and K. Hameyer, "Impact of cut edges in magnetization curves and iron losses in e-machines for automotive traction," in *Proc. 25th World Battery, Hybrid Fuel Cell Electr. Veh. Symp. Exhibit. (EVS)*, 2010.

[14] V. Maurel, F. Ossart, and R. Billardon, "Residual stresses in punched laminations: Phenomenological analysis and influence on the magnetic behavior of electrical steels," *J. Appl. Phys.*, vol. 93, no. 10, pp. 7106–7108, 2003.

[15] M. Bali, H. De Gersem, and A. Muetze, "Finite-element modeling of magnetic material degradation due to punching," *IEEE Trans. Magn.*, vol. 50, no. 2, article ID. 7018404, Feb. 2014.

[16] S. Steentjes, M. Leßmann, and K. Hameyer, "Advanced iron-loss calculation as a basis for efficiency improvement of electrical machines in automotive application," in *Proc. Electr. Syst. Aircraft, Railway Ship Propuls. (ESARS)*, 2012, pp. 1–6.

[17] S. Steentjes, M. Leßmann, and K. Hameyer, "Semi-physical parameter identification for an iron-loss formula allowing loss-separation," *J. Appl. Phys.*, vol. 113, no. 17, pp. 17A319-1–17A319-3, 2013.

[18] B. Hribernik, "Influence of cutting strains on the magnetic anisotropy of fully processed silicon steel," *J. Magn. Magn. Mater.*, vol. 26, nos. 1–3, pp. 72–74, 1982.